




## Transport properties of a quasisymmetric binary nitrogen-oxygen mixture in the warm dense regime

Yang-Shun Lan <sup>1,2</sup> Yun-Jun Gu,<sup>2</sup> Zhi-Guo Li <sup>2</sup> Guo-Jun Li,<sup>1,2</sup> Lei Liu,<sup>3</sup> Zhao-Qi Wang,<sup>4</sup> Qi-Feng Chen <sup>2,\*</sup> and Xiang-Rong Chen<sup>1,†</sup>

<sup>1</sup>College of Physics, Sichuan University, Chengdu 610064, People's Republic of China

<sup>2</sup>National Key Laboratory for Shock Wave and Detonation Physics Research, Institute of Fluid Physics, Chinese Academy of Engineering Physics, Mianyang 621900, People's Republic of China

<sup>3</sup>School of Science, Southwest University of Science and Technology, Mianyang 621010, China

<sup>4</sup>College of Science, Xi'an University of Science and Technology, Xi'an 710054, China



(Received 29 September 2021; accepted 14 December 2021; published 3 January 2022)

Transport properties of mixtures in the warm dense matter (WDM) regime play an important role in natural astrophysics. However, a physical understanding of ionic transport properties in quasisymmetric liquid mixtures has remained elusive. Here, we present extensive *ab initio* molecular dynamics (AIMD) simulations on the ionic diffusion and viscosity of a quasisymmetric binary nitrogen-oxygen (N-O) mixture in a wide warm dense regime of 8–120 kK and 4.5–8.0 g/cm<sup>3</sup>. Diffusion and viscosity of N-O mixtures with different compositions are obtained by using the Green–Kubo formula. Unlike asymmetric mixtures, the change of proportions in N-O mixtures slightly affects the viscosity and diffusion in the strong-coupling region. Furthermore, the AIMD results are used to build and verify a global pseudo-ion in jellium (PIJ) model for ionic transport calculations. The PIJ model succeeds in reproducing the transport properties of N-O mixtures where ionization has occurred, and provides a promising alternative approach to obtaining comparable results to AIMD simulations with relatively small computational costs. Our current results highlight the characteristic features of the quasisymmetric binary mixtures and demonstrate the applicability of the PIJ model in the WDM regime.

DOI: [10.1103/PhysRevE.105.015201](https://doi.org/10.1103/PhysRevE.105.015201)

### I. INTRODUCTION

Warm dense mixtures are ubiquitous in energy sources as well as in the interior of astronomical bodies [1–3]. The ionization properties of particles under these extreme circumstances vary between constituents, leading to extremely complex interactions and the diversity of the macroscopic properties, in particular, the transport properties [4]. The understanding of ionic transport in warm dense mixtures has recently become a topic of considerable interest [5,6]. Sedimentation of the neutron-rich isotope <sup>22</sup>Ne may be an important source of gravitational energy during the cooling of white-dwarf stars [7]. The segregation of hydrogen and helium in gas giant planets interiors such as Jupiter and Saturn [8–11], and the superionic state of hydrogen in ice giants such as Uranus and Neptune [chemical abundance ratio of hydrogen (H), carbon (C), nitrogen (N), and oxygen (O)] are crucial for modeling their interior structures [12–14]. Overall, it is vital to develop an accurate knowledge of ionic transport in warm dense mixtures.

It remains difficult to study experimentally the transport properties of warm dense mixtures. Thus, numerical simulation has become an extremely powerful tool that not only helps to understand experiments at the microscopic level

but also helps to study extreme conditions that are not accessible experimentally. Therefore, theoretical calculations are required to provide data on ionic transport coefficients. Currently, the widely used first-principles methods, including *ab initio* molecular dynamics (AIMD) [15–19] and orbital-free molecular dynamics (OFMD) [20–23], are able to obtain the ionic transport coefficients over a wide range of temperature and density. Note that the research is mainly directed at the asymmetric binary mixtures of H-He, H-C, H-Ag, etc., together with some multicomponent mixtures in the warm and hot dense matter regimes. More importantly, first-principles methods are often limited by expensive computational costs, especially for high temperatures that require a large number of bands. An effective alternative tool for calculating the transport parameters of mixtures at extremely high temperature-density conditions is the pseudo-ion in jellium (PIJ) model [22–24]. The backbone of the PIJ model combines two parts: Kinetic theory for particles and a coupled modeling to describe the interparticle interactions [21]. This model describes the ionization degree  $Q_i$  and coupling coefficient  $\Gamma_i$  of different particles in the mixtures, which effectively overcomes the problem of seeking an effective coupling parameter  $\Gamma_{\text{eff}}$  for the transport properties of mixtures in the one-component plasma (OCP) and Yukawa models [24]. For asymmetric mixtures, the PIJ model can reproduce many thermophysical parameters of warm dense matter (WDM) and dense plasmas, such as ionic transport coefficients and ion features [22,23]. However, the applicability of this model to

\*chenqf01@gmail.com

†xrchen@scu.edu.cn

symmetric mixtures in the WDM regime still needs to be further explored.

Quasisymmetric binary nitrogen-oxygen (N-O) mixtures are essential elemental components of detonation products and of some ice giant planets [3,25–28]. N-O mixtures under different concentrations have complicated structural and first-order properties under several thousand kelvins [29]. In detonation products and the deep interiors of planets, dissociation and ionization play a key role in N-O mixtures as the temperature increases, and the particles are in a mixed state. Here, we focus on the ionic transport properties of N-O mixtures at different concentrations to reveal a compositional effect. Whether the transport properties of quasisymmetric binary N-O mixtures will change significantly with concentration, like asymmetric mixtures, remains unknown.

In this work, extensive AIMD simulations are performed to explore the transport properties of N-O mixtures covering a wide temperature-density range of 8–120 kK and 4.5–8.0 g/cm<sup>3</sup>. Careful examination of the autocorrelation functions results in highly convergent diffusion and viscosity coefficients. Variable compositions (from 0% to 100%) are considered to reveal the compositional effect in the quasisymmetric N-O mixtures. To construct a PIJ model for binary N-O mixtures, hypernetted-chain equations are used to reproduce the structure of the mixture and derive the input of the global formulation of the transport coefficients. Finally, the PIJ model of N-O mixtures is validated by AIMD data. The present results not only fill the void in the research on thermophysical properties of binary N-O mixtures but also reveal the practicability of the PIJ model for quasisymmetric mixtures in the WDM regime.

## II. COMPUTATIONAL METHODS

### A. *Ab initio* molecular dynamics simulation

The AIMD simulations invoke the Born-Oppenheimer approximation to separate the electronic and ionic motions in which the force acting on ions is derived from an electronic calculation based on density functional theory, following which the ionic motion is described via Newton’s law, as implemented in the VASP package [30]. Exchange-correlation effects are approximated with a zero-temperature model of the Perdew-Burke-Ernzerhof functional [31]. The  $2s^22p^3$  electrons of N and  $2s^22p^4$  electrons of O are explicitly treated as valence electrons, the electronic wave functions are expanded in a plane wave basis with an energy cutoff of 800 eV, with core electrons represented by pseudopotentials of the projector augmented wave type [32]. The number of electrons is compatible with the total number derived from the valence in all atoms to assure charge neutrality. The  $\Gamma$  point is used to sample the Brillouin zone, and the simulation supercell contains 90 atoms in a cubic box with boundary conditions, periodically replicated throughout space in a consistent manner. The MD simulations are performed within the canonical (NVT) ensemble, where a Nosé–Hoover thermostat [33] is coupled to the ionic degrees of freedom and electronic states are populated according to the Fermi-Dirac distribution [34]. Seven different mixing ratios ( $x_O = 0\%$ , 25%, 33.3%, 50%, 66.6%, 75%, and 100%) are considered in this work to explore

the compositional effect. The simulation supercell contains 90 atoms in a cubic box, and we typically run for 20 000 steps for each  $\rho$ - $T$  condition. The time step covers 0.25–1.0 fs and smaller values correspond to higher temperatures. Considering the crucial role of spin fluctuations present in liquid oxygen [35], the spin-polarization effect is included in the present AIMD calculation of N-O mixtures. The spin-polarization affects the microscopic structure of the N-O mixtures, as shown in Fig. S1 of the Supplemental Material (SM) [36], and ignoring spin polarization will underestimate the pair correlation functions  $g(r)$ . Additionally, the extensive convergence tests are carefully carried out to ensure the reliability of these selected parameters, which will be presented below.

The self-diffusion coefficient of a particular ion species  $D_\alpha$  is extracted from the integral of the velocity autocorrelation function (VACF) by using the Green-Kubo formula [37],

$$D_\alpha = \frac{1}{3} \int_0^\infty \langle \vec{v}_i(t) \cdot \vec{v}_i(0) \rangle dt, \quad (1)$$

where  $v_i(t)$  is the velocity of the  $i$ th particle ( $\alpha$  species) at time  $t$ , and the bracket indicates an ensemble average. Similarly, mutual-diffusion coefficients are found within the Maxwell–Stefan formula through the integral of the mutual-diffusion current autocorrelation function (MCACF):

$$D_{\alpha\beta} = \frac{1}{3N x_\alpha x_\beta} \int_0^\infty \langle A(t)A(0) \rangle dt, \quad (2)$$

$$A(t) = x_\beta \sum_i^{N_\alpha} \vec{v}_i(t) - x_\alpha \sum_j^{N_\beta} \vec{v}_j(t), \quad (3)$$

where  $A(t)$  is the mutual-diffusion current,  $N$  is the total number of particles, and  $x_\alpha$  is the concentration of component  $\alpha$ . The shear viscosity  $\eta$  can be determined by the stress tensor autocorrelation function (STACF) [37],

$$\eta = \frac{V}{k_B T} \int_0^\infty \langle P_{ij}(t')P_{ij}(0) \rangle dt', \quad (4)$$

where  $V$ ,  $k_B$ , and  $T$  are the volume, Boltzmann constant, and temperature, respectively.  $P_{ij}(t)$  represents the averaged result for five independent off-diagonal components of the stress tensor:  $P_{xy}$ ,  $P_{yz}$ ,  $P_{zx}$ ,  $(P_{xx} - P_{yy})/2$ , and  $(P_{yy} - P_{zz})/2$ . To overcome the limited simulation time of AIMD and noise in the long-time behavior of ACFs, an appropriate fitting method of the ACFs by Meyer *et al.* [38] and Guo *et al.* [39] is adopted to yield the ionic transport properties; see details in the SM [36].

### B. Hypernetted-chain equations

The weak-coupling approximation fails for WDM and strongly coupled plasmas, where the correlations cannot be treated as a small perturbation of the thermal motion [40–43]. Here, the modeling of the static structure within higher-order correlations can be implemented by the multi-component extension of the integral equation of fluid theory, the hypernetted-chain theory (HNC) [44]. For binary ionic mixture, the integral equations approach starts with the general Ornstein–Zernike relation that describes the total pair

correlation function  $h_{\alpha\beta}(r)$  and direct correlation functions  $c_{\alpha\beta}(r)$  [45–47],

$$h_{\alpha\beta}(r) = c_{\alpha\beta}(r) + \sum_{\lambda} n_{\lambda} \int c_{\alpha\lambda}(|\mathbf{r} - \mathbf{r}'|) h_{\lambda\beta}(r') d\mathbf{r}'. \quad (5)$$

Furthermore, the exact expression of the pair distribution functions  $g_{\alpha\beta}(r)$  is needed to fully determine the closure relation of the HNC:

$$g_{\alpha\beta}(r) = \exp \left[ -\frac{V_{\alpha\beta}(r)}{k_B T} + h_{\alpha\beta}(r) - c_{\alpha\beta}(r) + B_{\alpha\beta}(r) \right], \quad (6)$$

where  $h_{\alpha\beta}(r) = g_{\alpha\beta}(r) - 1$ . In the strongly coupled region, the interaction between species  $\alpha$  and  $\beta$  is expressed by the Coulomb potential  $V_{\alpha\beta}(r) = Q_{\alpha} Q_{\beta} e^2 / r$ , where  $Q_{\alpha}$  is the ion charge state of component  $\alpha$ ,  $e$  is the fundamental charge, and  $B_{\alpha\beta}(r)$  is the bridge function. For the numerical evaluation, the Ornstein–Zernike relation contains a convolution, so it is an algebraic matrix equation in Fourier space,

$$\tilde{h}_{\alpha\beta} = \tilde{c}_{\alpha\beta} + \sum_i n_i \tilde{c}_{\alpha i} \tilde{h}_{i\beta}, \quad (7)$$

where  $n_i$  is the density of the species  $i$ .

The HNC approximation ignores the contributions arising from the potential of mean force in the logarithm of the radial-distribution function, especially in the strong-coupling system, while the bridge functions  $B_{\alpha\beta}(r)$  account for strong correlations at short distances.  $B_{\alpha\beta}(r)$  is used to modify the HNC approximation breakdown in the vicinity of the first peak of  $g(r)$  [48–50],

$$B_{ii}(r) = -0.0464 \Gamma^{1.336} \exp \left( -\frac{b_1}{b_0} r^2 \right), \quad (8)$$

$$\begin{aligned} b_0 &= 0.258 - 0.0612 \ln \Gamma + 0.0123 (\ln \Gamma)^2 - 1/\Gamma, \\ b_1 &= 0.0269 + 0.0318 \ln \Gamma + 0.00814 (\ln \Gamma)^2, \end{aligned} \quad (9)$$

where  $\Gamma = \sqrt{\Gamma_{\alpha} \Gamma_{\beta}}$  and  $\Gamma_{\alpha}$  is the coupling coefficient of component  $\alpha$ . The coupling parameter  $\Gamma_{\alpha}$  is defined by  $\Gamma_{\alpha} = Q_{\alpha}^2 e^2 / (a_{\alpha} k_B T)$ , where  $a_{\alpha} = (3/4\pi n_{\alpha})^{1/3}$  is the mean ion sphere, and  $n_{\alpha}$  is the ionic density.

### C. Pseudo-ion in jellium model

The PIJ model, which assumes that the electron screening on ion-ion interactions can be accounted for by considering pointlike pseudo-ions interacting in a jellium, addresses the viscosity and diffusion of extensive asymmetric WDM and plasmas of pure elements and multicomponent mixtures [21,24]. The model treats on an equal footing both strongly and weakly coupled regimes, and the main idea is to gather, in a single scheme, approximate kinetic expressions and coupled evaluations of transport coefficients reflecting the thermodynamic state of the mixture. The ionic transport in mixtures is

$$\eta = \eta^{\text{FPL}} + \eta_{\text{ex}}, \quad (10)$$

$$D = D^{\text{FPL}} + D_{\text{ex}}. \quad (11)$$

In the kinetic regime, transport coefficients are given using collision frequency estimates in the Fokker-Planck-Landau framework (FPL) [51,52],

$$\eta^{\text{FPL}} = K_1 \frac{n_{\alpha} k_B T}{\tilde{v}_{\alpha}} + K_2 \frac{n_{\beta} k_B T}{\tilde{v}_{\beta}}, \quad (12)$$

$$D_{\alpha\beta}^{\text{FPL}} = R_{12} c_{\beta} \frac{k_B T}{v_{\alpha\beta}} \frac{\bar{m}}{m_{\alpha} m_{\beta}}, \quad (13)$$

$$D_i^{\text{FPL}} = R_{\alpha} \frac{1}{\tilde{v}_i} \frac{k_B T}{m_i}, \quad i = \alpha, \beta, \quad (14)$$

where  $m_{\alpha}$  is the mass of component  $\alpha$ ,  $c_{\alpha}$  is its mass concentration, and  $\bar{m} = x_{\alpha} m_{\alpha} + x_{\beta} m_{\beta}$  is the effective mass.  $K_1$ ,  $K_2$ ,  $R_1$ ,  $R_2$ , and  $R_{12}$  are correction factors, which are evaluated by solving the linearized kinetic equations to obtain the corrections to the Maxwellian distributions associated with small gradients of density, velocity, and temperature [53,54]. In the moderate- to strong-coupling regime of the present cases,  $R_1 = R_2 = R_{12} = 1.19$  and  $K_1 = K_2 = 0.965$  is suggested by Ticknor *et al.* [22], which is effectively applied to asymmetric mixtures in the WDM range. The collision frequency between two fully ionized charged elements is

$$v_{\alpha\beta} = \frac{n_{\beta}}{m_{\alpha}} \frac{4\sqrt{2\pi} m_{\alpha\beta} Q_{\alpha}^2 Q_{\beta}^2 e^4 \ln \Lambda_{\alpha\beta}}{3(k_B T)^{3/2}}, \quad (15)$$

where  $m_{\alpha\beta} = m_{\alpha} m_{\beta} / (m_{\alpha} + m_{\beta})$  is the reduced mass, and  $\ln \Lambda_{\alpha\beta}$  is the Coulomb logarithm for binary collisions between species  $\alpha$  and  $\beta$  [55],

$$\ln \Lambda_{\alpha\beta} = \ln \left( \frac{b_{\alpha\beta}^{\text{max}}}{b_{\alpha\beta}^{\text{min}}} \right), \quad (16)$$

where the minimum impact parameter  $b^{\text{min}}$  is given by the classical formula for ions,  $b_{\alpha\beta}^{\text{min}} = Q_{\alpha} Q_{\beta} e^2 / (2k_B T)$ , and the maximum impact parameter  $b^{\text{max}}$  is given by the Debye length for ions,  $b_{\alpha\beta}^{\text{max}} = (4\pi n \langle Q^2 \rangle e^2 / k_B T)^{-1/2}$ , where  $\langle Q \rangle = \sum_{\alpha} x_{\alpha} Q_{\alpha}$  is the average charge. The total collision frequencies for each species are  $\tilde{v}_{\alpha} = v_{\alpha\alpha} + v_{\alpha\beta}$  and  $\tilde{v}_{\beta} = v_{\beta\beta} + v_{\beta\alpha}$ . In the strong-coupling regime, bounded Coulomb logarithms are required to avoid divergence:  $\ln \Lambda = \max(\ln \Lambda, L_0)$  with  $L_0 = 3.00$ .

In the coupled regime, the mixing rules are used to estimate the excess contributions  $D_{\text{ex}}$  and  $\eta_{\text{ex}}$ . For the viscosity, an equivalent OCP with charge  $Q_{\text{eff}}$  is defined, corresponding to the effective coupling  $\Gamma_{\text{eff}}$  of the mixture, and evaluate  $\eta_{\text{ex}}$  as

$$\eta_{\text{ex}} = \eta_{\text{OCP}}(\Gamma_{\text{eff}}, \rho, T) - \eta_{\text{FPL}}(\Gamma_{\text{eff}}, \rho, T), \quad (17)$$

where the  $\Gamma_{\text{eff}}$  is equal to

$$\Gamma_{\text{eff}} = \sum_{\alpha} x_{\alpha} \Gamma_{\alpha} = \frac{\langle Q^{5/3} \rangle \langle Q \rangle^{1/3}}{a k_B T}. \quad (18)$$

For self-diffusion, the excess contributions  $D_{\alpha,\text{ex}}$  is defined as

$$D_{\alpha,\text{ex}} = D_{\text{OCP}}(\Gamma_{\alpha}, \rho_{\alpha}, T) - D_{\text{FPL}}(\Gamma_{\alpha}, \rho_{\alpha}, T), \quad (19)$$

and the Darken relation is applied in the limit of excess mutual-diffusion,

$$D_{\alpha\beta,\text{ex}} = x_{\alpha} D_{\beta,\text{ex}} + x_{\beta} D_{\alpha,\text{ex}}. \quad (20)$$

In the FPL framework, the viscosity  $\eta_{\text{FPL}}$  and self-diffusion  $D_{\text{FPL}}$  are given by  $\eta_{\text{FPL}} = 0.557\pi^{1/2} \Gamma^{-5/2} / \ln \Lambda$  and  $D_{\text{FPL}} =$

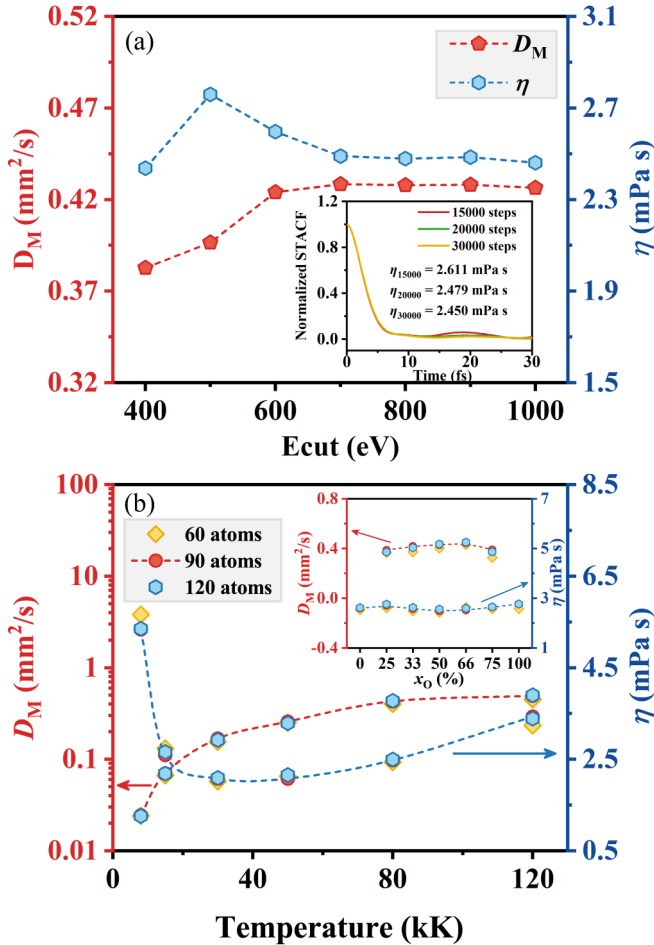


FIG. 1. The (a) energy cutoff and (b) supercell convergence tests of mutual-diffusion coefficients  $D_M$  and viscosity  $\eta$  for  $x_O = 50\%$  at  $8.0 \text{ g/cm}^3$ . The inset of panel (a) shows the convergence of normalized STACF with respect to the simulation steps. The inset of panel (b) shows the convergence test of transport properties under different concentrations at  $8.0 \text{ g/cm}^3$  and  $80 \text{ kK}$ .

$1.234\eta_{\text{FPL}}$ , respectively. For OCP diffusion and viscosity, the empirical function of Daligault *et al.* [56] and Bastea *et al.* [57] are used, and a smooth transition across coupling regimes is then achieved at  $\Gamma \approx 0.15$ .

### III. RESULTS AND DISCUSSION

First, detailed convergence tests on the simulation parameters including cutoff energy, simulation step, and size of supercell are performed, which is essential for accessing reliable ionic velocity and force. Figure 1(a) presents the convergence test of cutoff energy and simulation step. Note that relaxation times of the autocorrelation functions under different oxygen concentrations are close, so only the test results for a typical ratio ( $x_O = 50\%$ ) are shown. The test results of cutoff energy show that  $700 \text{ eV}$  can make diffusion and viscosity converge to  $0.7\%$ . Diffusions and viscosities require very long trajectories to arrive at desirably convergent values, especially for viscosities. The stress tensor is the property of the entire system without an additional average over  $N_\alpha$  particles, so the viscosity is subjected to greater statistical imprecision than

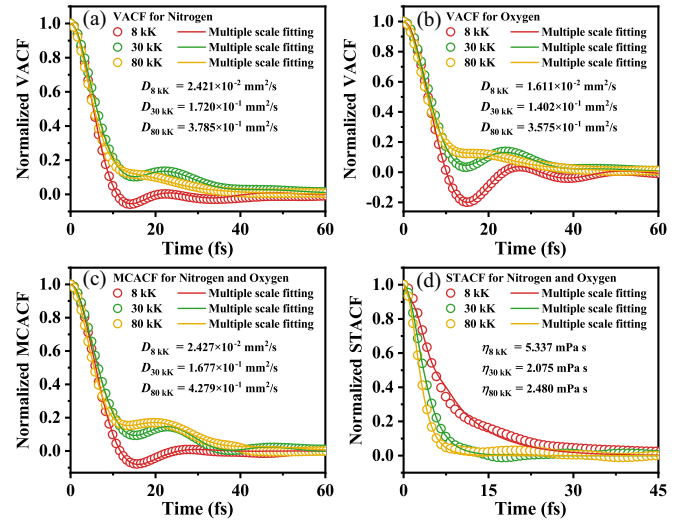


FIG. 2. Normalized ACFs of N-O mixtures with  $x_O = 50\%$  ( $8.00 \text{ g/cm}^3$ ) at three representative temperatures. The present AIMD data (symbols) are compared with the fitting results (solid lines) by using a multiple-timescale function, and the corresponding results are  $D$  and  $\eta$ , respectively.

the diffusion coefficient [9,15]. Consequently, convergence tests of time steps for normalized STACFs are given in the inset of Fig. 1(a). One can clearly see that the deviation of the viscosity coefficient between 15 000 and 30 000 steps is larger than  $6\%$ , while that for 20 000 and 30 000 steps is only  $1.2\%$ . The tests of the finite-size effect taking into account the influence of temperature and concentration are performed using 60, 90, and 120 atoms, as shown in Fig. 1(b). The results with 60 atoms deviate up to  $7\%$  from those with 120 atoms, while the results with 90 and 120 atoms show good consistency. Therefore, supercells with 90 atoms and 20 000 simulation steps are sufficient to obtain converged results.

The time ACFs are of great interest in computational simulations due to their clear picture of dynamics in a fluid system. To explore how different ionic structures affect the dynamical behavior of N-O mixtures, normalized ACFs of N-O mixtures with  $x_O = 50\%$  ( $8.00 \text{ g/cm}^3$ ) at three representative temperatures are shown in Fig. 2. The VACFs and MCACFs are used to determine the diffusion coefficients, as shown in Figs. 2(a)–2(c). The negative correlation regions and oscillatory features are evident on VACFs and MCACF at  $8 \text{ kK}$ , which is an embodiment of the bonding effect. This phenomenon can also be understood from  $g(r)$  in Fig. S2 [36]. The obvious peaks in  $g(r)$  indicate the rich bonding structures in N-O mixtures at  $8 \text{ kK}$ , and the bonding structures have negative contributions to the atomic transport. The bonding system structures undergo violent dissociation as the temperature rises. The oscillation of the correlation functions at elevated temperatures, such as  $30 \text{ kK}$ , is mainly caused by the cage effect. As the temperature increases, the short- and medium-range order fluid states are destroyed, weakening the cage effect. The STACFs decay to zero in a few tens of femtoseconds, as shown in Fig. 2(d), and the normalized STACFs tend to attenuate monotonically as the temperature increases. As suggested by Meyer *et al.* [38] and Guo *et al.* [39], the

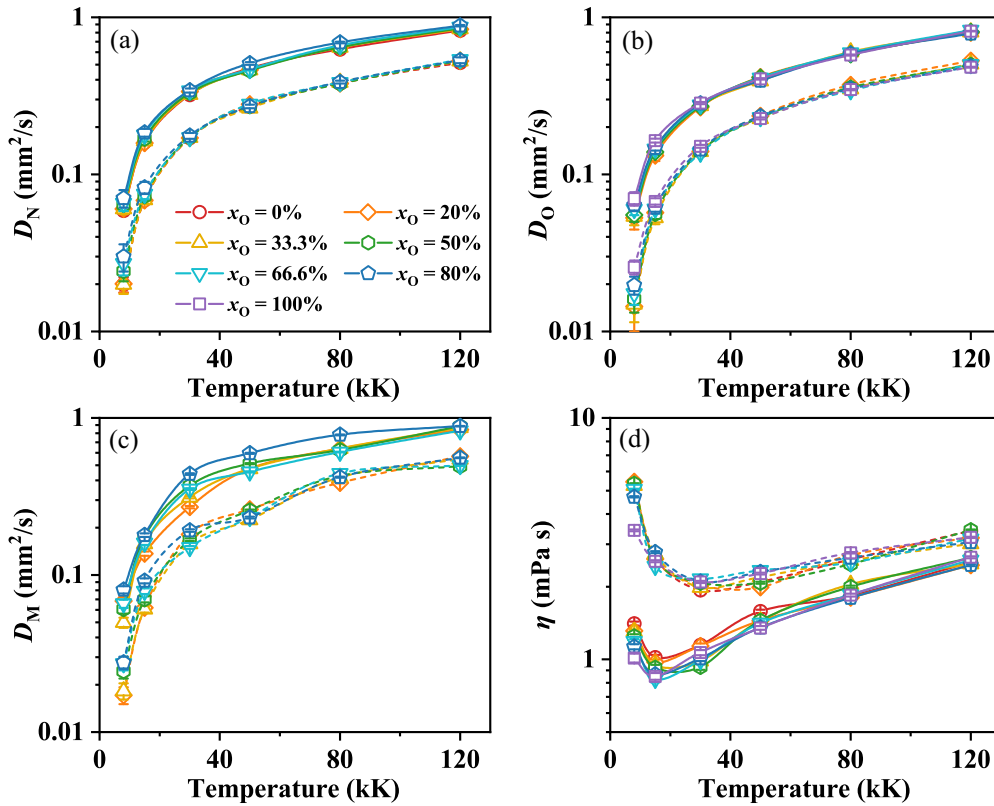


FIG. 3. The self-diffusion for (a) nitrogen  $D_N$  and (b) oxygen  $D_O$ , (c) mutual-diffusion  $D_M$ , and (d) viscosity  $\eta$  coefficients of N-O mixtures obtained by AIMD simulation along the isochores for densities 4.50 (solid lines) and 8.00 g/cm<sup>3</sup> (dashed lines) and temperatures between 8 and 120 kK.

diffusion and viscosity coefficients of the N-O mixture can be estimated by using exponential-decay functions to fit the ACFs. Note that the fits go smoothly through ACFs data points for different temperatures, and the ionic transport properties can be obtained by numerical analytical expressions. Detailed descriptions of the fitting method used to derive the transport coefficients are provided in the SM [36]. The normalized ACFs of N-O mixtures under different concentrations are also shown in Fig. S4 [36]. The ionic transport coefficients of N-O mixtures under different proportions are obtained by using the same method as above.

The derived diffusion and viscosity coefficients of N-O mixtures at densities of 4.5 and 8.0 g/cm<sup>3</sup> and temperatures from 8 to 120 kK are presented in Fig. 3. As shown in Figs. 3(a)–3(c), both self- and mutual-diffusions in N-O mixtures become larger as the temperature increases because the heat velocities get higher. Simultaneously, at a certain temperature, the diffusion coefficients decrease as the density increases, which is caused by the stronger general interactions between fluid particles at higher densities. Unlike asymmetric mixtures, such as H-C and H-Ag mixtures [22,23], the diffusion coefficients of N-O mixtures, especially self-diffusions, do not change significantly with concentration. Moreover, the calculated viscosity coefficients of N-O mixtures are displayed in Fig. 3(d). The viscosity increases with density, and seems to have a local minimum within the present temperature range. That is because the viscosity arises from the transport of momentum, which is related to not only the

bodily movement of particles but also the mean free path of particles [9,18]. The probabilities of particle mixing and collision increase as the temperature rises, which decreases the mean free path of particles and reduces the viscosity. On the other hand, the velocity of ionic motion increases as the temperature rise, resulting in intensified momentum exchange and increased the viscosity. The two mechanisms have a competitive relation as the temperature increases, which leads to the viscosity perhaps having a local minimum as a function of temperature. However, the concentration effect does not significantly change the momentum transmission of the N-O system, and the viscosity has a similar performance with diffusion coefficients under the change of concentration. The present AIMD simulations give accurate ionic transport information on N-O mixtures, which exhibit characteristics different from asymmetric mixtures and can be used to benchmark the PIJ models for quasisymmetric mixtures in the WDM regime.

The PIJ model provides a highly desirable, alternative method to predict the transport coefficients. In this concept, it is of primary importance to determine the coupling coefficients  $\Gamma_i$  for each species. The input of the global PIJ model can be found by using the  $g(r)$  as an indicator of the existence of these correlations and then matching the  $g(r)$  of HNC to that of AIMD. To obtain a fast evaluation of the  $g(r)$  for the HNC, the initial values of  $\Gamma_i$  are estimated using the Thomas–Fermi approximation [58]. For each thermodynamic state, we use an iterative method to search for the  $\Gamma_i$  of HNC by finding

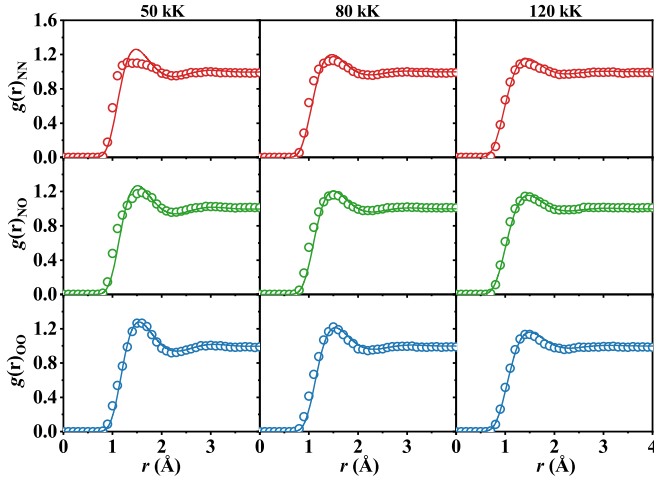


FIG. 4. Comparison of pair correlation functions  $g(r)$  obtained by AIMD simulations (symbols) with HNC calculations (solid lines) in a N-O mixture ( $x_O = 50\%$ ) for densities of  $8.00 \text{ g/cm}^3$  and temperatures between 50 and 120 kK.

the best agreement with AIMD in terms of the distance of closest approach, position of the main peak, and the first minimum of  $g(r)$ . Figure 4 plots the  $g(r)$  of the N-O mixtures with  $x_O = 50\%$  under different temperatures. Except for  $g(r)_{NN}$  at 50 kK, the HNC results perfectly fit the AIMD simulation. This effect naturally lies in the ability of N to adopt different bond types (single to triple) [29,59], which forces the nitrogen atoms to be distributed within a certain distance and leads to the multipeak characteristics in  $g(r)_{NN}$ . The HNC equations with only Coulombic correlations cannot match the AIMD's  $g(r)$  with multipeak characteristics, so it becomes no longer applicable below 50 kK. As the temperature increases, the main peak of  $g(r)$  becomes inconspicuous, which shows that the coupling coefficients of particles decrease and the ionization increases with temperature. The similar structure of each  $g(r)$  in the N-O system implies that, at the same temperature, the coupling coefficient and ionization of N and O particles are close. The  $g(r)$  of N-O mixtures under different concentrations at 80 and 120 kK are also presented in Fig. S5 [36]. Interestingly, the correlations between the particles in the quasisymmetric N-O system are weakly affected by the concentrations, which indicates that, compared with the asymmetric mixture, the coupling coefficients and ionization of particles change slightly with concentration. Taking into account the screening effect in the system, the HNC with the Yukawa-type interaction is also used to calculate  $g(r)$ , which is compared with the  $g(r)$  calculated by the Coulomb-type interaction, as shown in Fig. S6 [36]. Under the same coupling coefficients, the  $g(r)$  obtained by the HNC with the Yukawa-type interaction and the Coulomb-type interaction differ only slightly, and both provide a better match for the  $g(r)$  of AIMD.

To gain further insight into the ionization effect, the electronic density of states as a function of temperature and density in N-O mixtures are exhibited in Fig. S7 [36]. Both temperature and pressure affect in the area above 30 kK will contribute to ionization. Combining the above matching  $g(r)$  of HNC and AIMD, only the ionization states with temperatures above 80 kK are considered in our current PIJ model

TABLE I. Representative coupling coefficient  $\Gamma_\alpha$  of each species and effective coupling coefficient  $\Gamma_{\text{eff}}$  and ionization  $Q_{\text{eff}}$  of the N-O mixtures with  $x_O = 50\%$  by matching the  $g(r)$  of HNC calculations with the results of AIMD. For comparison, the ionization  $Q_{\text{S-D}}$  obtained by Smith-Drude model is also listed.

$\rho(\text{g/cm}^3)$	$T(\text{kK})$	$\Gamma_N$	$\Gamma_O$	$\Gamma_{\text{eff}}$	$Q_{\text{eff}}$	$Q_{\text{S-D}}$
4.50	80	8.70	9.90	9.30	2.209	2.703
	120	7.50	8.20	7.85	2.487	2.992
8.00	80	14.00	18.00	16.00	2.630	3.186
	120	11.80	14.20	13.00	2.906	3.331

for N-O mixtures. Table I lists the coupling coefficients and effective ionization of the N-O mixtures with  $x_O = 50\%$ , which are obtained by matching the  $g(r)$  of HNC calculations to that of the AIMD simulations. At the same time, the effective ionization of the AIMD simulation obtained via the Smith-Drude model [60] is also given for comparison. Here, the Smith-Drude model is used to fit the real part of the frequency-dependent conductivity to obtain the delocalized electron density  $n_e$  (a representative fit can be found in Fig. S8 [36]), and the ionization state  $Q_{\text{S-D}}$  of N-O mixtures can be estimated by  $n_e/n_{\text{tot}}$ , where  $n_{\text{tot}}$  is the ionic density of the system, see details in the SM [36]. Both the ionization calculated by HNC and by the Smith-Drude model indicate a feature of strongly correlated particles in the N-O mixtures at the temperatures used. The ionization increases with increasing temperature and density. The ionization states produced by these two methods are in general agreement with each other, but an accurate theoretical determination of this parameter in the WDM regime remains an open question. The Smith-Drude model only gives the effective ionization of the system, while the HNC calculations can give the coupling parameters of each species in N-O mixtures ranging from 7.5 to 18, which can be used as an input to predict the transport coefficients in the PIJ Model.

The transport coefficients for N-O mixtures obtained with different concentrations by the PIJ model are compared with AIMD results in Fig. 5. The self-diffusion coefficients of N and O obtained by both the PIJ model and AIMD simulation remain essentially constant as the proportion of O elements varies, as shown in Figs. 5(a) and 5(b). The coupling coefficients of the particles are close and the collision frequency does not change significantly in the quasisymmetric N-O system, which is definitely different from the asymmetric mixtures [22,23]. In our temperature scope, the PIJ model predicts reasonably well the results of AIMD at the low density corresponding to a small coupling coefficient, whereas the diffusion of nitrogen is overestimated at high density. In contrast with the self-diffusion coefficients, the mutual-diffusion coefficients change more obviously with concentration, as shown in Fig. 5(c). The mutual-diffusion in the PIJ model follows the behavior predicted by the Darken relation, interpolating between the self-diffusion of N and O. The Darken relation broadly approximates to the mutual diffusion, with deviations typically within 7% of the AIMD results at low density, but is no longer effective at high density due to overestimation of the self-diffusion of nitrogen. For viscosity [Fig. 5(d)], the PIJ

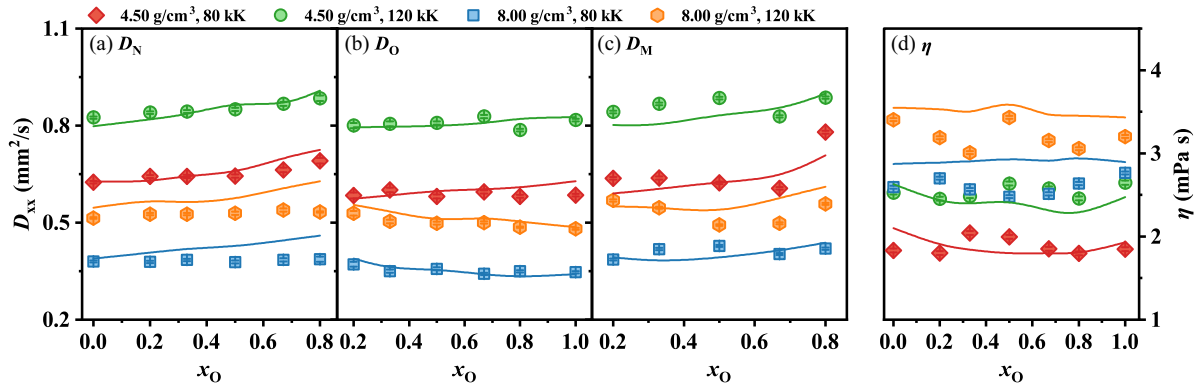


FIG. 5. Comparison of AIMD simulations (symbols) with the PIJ model (solid lines) for ionic transport properties in N-O mixtures under different concentrations: Self-diffusion for (a) nitrogen  $D_N$  and (b) oxygen  $D_O$ , (c) mutual-diffusion  $D_M$ , and (d) viscosity  $\eta$ .

model shows not globally well agreement with the results of AIMD. The PIJ model significantly overestimates the viscosity, and the maximum deviations at low density reach 10%. Our current results show that the PIJ model provides, to some extent, an effective alternative approach with relatively small computational costs to calculating the diffusion of warm dense N-O systems in the strong-coupling region, and the viscosity obtained by the PIJ model requires careful consideration due to larger deviations.

#### IV. CONCLUSIONS

We perform extensive AIMD simulations to explore the transport properties of N-O mixtures with various proportions (from 0% to 100%) in the WMD regime. The numerically converged self-diffusion and mutual-diffusion generally increase with temperature, and the viscosity increases with density and has a local minimum in the present temperature range. Unlike asymmetric mixtures, the diffusion and viscosity coefficients show no significant dependence on the concentration of elemental oxygen. The HNC equations give the method of searching for the coupling parameters and the global input of PIJ models, and the AIMD results are then used as a benchmark to validate the present PIJ models. The

PIJ model successfully reproduced these transport properties where ionization has occurred, which shows broadly consistent with the diffusions of AIMD at the low density. It provides an effective alternative way to determine the ionic transport coefficients of N-O mixtures with reduced AIMD computational cost. These results reveal that the transport properties of quasisymmetric mixtures are not as sensitive to concentration as symmetric mixtures, and demonstrate the PIJ model to be a possible way to determine the transport coefficient of quasisymmetric mixtures in the WDM region. Besides binary quasisymmetric mixtures, it is our intention to show in future work how these mixing processes of ternary quasisymmetric mixtures, such as C-N-O mixtures, directly simulate and model the deep interiors of planets.

#### ACKNOWLEDGMENTS

This work is supported by the National Natural Science Foundation of China (Grants No. 11872057 and No. 12074274), and the Foundation of National Key Laboratory of Shock Wave and Detonation Physics (Grant No. JCYKS2020212009). We also acknowledge the support for the computational resources of the Shanghai Supercomputer Center in China.

- [1] R. Betti and O. A. Hurricane, *Nat. Phys.* **12**, 435 (2016).
- [2] P. E. Tremblay and P. Bergeron, *Astrophys. J.* **672**, 1144 (2008).
- [3] M. S. Lee and S. Scandolo, *Nat. Commun.* **2**, 185 (2011).
- [4] V. A. Smalyuk, L. J. Atherton, L. R. Benedetti, R. Bionta, D. Bleuel, E. Bond, D. K. Bradley, J. Caggiano, D. A. Callahan, D. T. Casey, P. M. Celliers, C. J. Cerjan, D. Clark, E. L. Dewald, S. N. Dixit, T. Doppner, D. H. Edgell, M. J. Edwards, J. Frenje, M. Gatu-Johnson *et al.*, *Phys. Rev. Lett.* **111**, 215001 (2013).
- [5] J. Daligault, S. D. Baalrud, C. E. Starrett, D. Saumon, and T. Sjostrom, *Phys. Rev. Lett.* **116**, 075002 (2016).
- [6] S. Gopalakrishnan and R. Vasseur, *Phys. Rev. Lett.* **122**, 127202 (2019).
- [7] J. Hughto, A. S. Schneider, C. J. Horowitz, and D. K. Berry, *Phys. Rev. E* **82**, 066401 (2010).
- [8] D. Bruno, C. Catalfamo, M. Capitelli, G. Colonna, O. De Pascale, P. Diomede, C. Gorse, A. Laricchiuta, S. Longo, D. Giordano, and F. Pirani, *Phys. Plasmas* **17**, 112315 (2010).
- [9] Z.-G. Li, W. Zhang, Z.-J. Fu, J.-Y. Dai, Q.-F. Chen, and X.-R. Chen, *Phys. Plasmas* **24**, 052903 (2017).
- [10] F. Soubiran, B. Militzer, K. P. Driver, and S. Zhang, *Phys. Plasmas* **24**, 041401 (2017).
- [11] G.-J. Li, Z.-G. Li, Q.-F. Chen, Y.-J. Gu, W. Zhang, L. Liu, H.-Y. Geng, Z.-Q. Wang, Y.-S. Lan, Y. Hou, J.-Y. Dai, and X.-R. Chen, *Phys. Rev. Lett.* **126**, 075701 (2021).
- [12] C. Ticknor, L. A. Collins, and J. D. Kress, *Phys. Rev. E* **92**, 023101 (2015).
- [13] R. Chau, S. Hamel, and W. J. Nellis, *Nat. Commun.* **2**, 203 (2011).
- [14] R. Helled, N. Nettelmann, and T. Guillot, *Space Sci. Rev.* **216**, 00660 (2020).

- [15] L. Liu, Z. G. Li, J. Y. Dai, Q. F. Chen, and X. R. Chen, *Phys. Rev. E* **97**, 063204 (2018).
- [16] F. Lambert and V. Recoules, *Phys. Rev. E* **86**, 026405 (2012).
- [17] C. Wang, Y. Long, X. T. He, J. F. Wu, W. H. Ye, and P. Zhang, *Phys. Rev. E* **88**, 013106 (2013).
- [18] Z. Q. Wang, J. Tang, Y. Hou, Q. F. Chen, X. R. Chen, J. Y. Dai, X. J. Meng, Y. J. Gu, L. Liu, G. J. Li, Y. S. Lan, and Z. G. Li, *Phys. Rev. E* **101**, 023302 (2020).
- [19] J. Dai, Y. Hou, D. Kang, H. Sun, J. Wu, and J. Yuan, *New J. Phys.* **15**, 045003 (2013).
- [20] A. J. White, C. Ticknor, E. R. Meyer, J. D. Kress, and L. A. Collins, *Phys. Rev. E* **100**, 033213 (2019).
- [21] J. Clerouin, P. Arnault, B. J. Grea, S. Guisset, M. Vandenboomgaerde, A. J. White, L. A. Collins, J. D. Kress, and C. Ticknor, *Phys. Rev. E* **101**, 033207 (2020).
- [22] C. Ticknor, J. D. Kress, L. A. Collins, J. Clerouin, P. Arnault, and A. Decoster, *Phys. Rev. E* **93**, 063208 (2016).
- [23] A. J. White, L. A. Collins, J. D. Kress, C. Ticknor, J. Clerouin, P. Arnault, and N. Desbiens, *Phys. Rev. E* **95**, 063202 (2017).
- [24] P. Arnault, *High Energy Density Phys.* **9**, 711 (2013).
- [25] N. Nettelmann, K. Wang, J. J. Fortney, S. Hamel, S. Yellamilli, M. Bethkenhagen, and R. Redmer, *Icarus* **275**, 107 (2016).
- [26] C. Dalou, M. M. Hirschmann, A. von der Handt, J. Mosenfelder, and L. S. Armstrong, *Earth Planet. Sci. Lett.* **458**, 141 (2017).
- [27] X. Jiang, G. Chen, X. Cheng, Y. Li, and F. Guo, *J. Phys. Chem. C* **120**, 13366 (2016).
- [28] N. Goldman and S. Bastea, *J. Phys. Chem. A* **118**, 2897 (2014).
- [29] Y.-S. Lan, Z.-Q. Wang, L. Liu, G.-J. Li, H.-Y. Sun, Z.-J. Fu, Y.-J. Gu, G. Yang, L.-N. Li, Z.-G. Li, Q.-F. Chen, and X.-R. Chen, *Phys. Rev. B* **103**, 144105 (2021).
- [30] G. Kresse and J. Furthmuller, *Phys. Rev. B* **54**, 11169 (1996).
- [31] J. P. Perdew, K. Burke, and M. Ernzerhof, *Phys. Rev. Lett.* **77**, 3865 (1996).
- [32] P. E. Blöchl, *Phys. Rev. B* **50**, 17953 (1994).
- [33] S. Nosé, *J. Chem. Phys.* **81**, 511 (1984).
- [34] N. D. Mermin, *Phys. Rev.* **137**, A1441 (1965).
- [35] B. Militzer, F. Gygi, and G. Galli, *Phys. Rev. Lett.* **91**, 265503 (2003).
- [36] See Supplemental Material at <http://link.aps.org/supplemental/10.1103/PhysRevE.105.015201> for results of pair correlation functions  $g_r$ , autocorrelation function, structure comparison of hypernetted chain equations and AIMD simulations, and electronic density of states and ionization, which includes Refs. [61–66].
- [37] M. P. Allen and D. J. Tildesley, *Computer Simulation of Liquids* (Oxford University Press, Oxford, 2017).
- [38] E. R. Meyer, J. D. Kress, L. A. Collins, and C. Ticknor, *Phys. Rev. E* **90**, 043101 (2014).
- [39] G.-J. Guo, Y.-G. Zhang, K. Refson, and Y.-J. Zhao, *Mol. Phys.* **100**, 2617 (2002).
- [40] J. F. Springer, M. A. Pokrant, and F. A. Stevens, *J. Chem. Phys.* **58**, 4863 (1973).
- [41] K. Ng, *J. Chem. Phys.* **61**, 2680 (1974).
- [42] K. Wunsch, J. Vorberger, and D. O. Gericke, *Phys. Rev. E* **79**, 010201(R) (2009).
- [43] R. Bredow, T. Bornath, W. D. Kraeft, and R. Redmer, *Contrib. Plasma Phys.* **53**, 276 (2013).
- [44] K. Wunsch, P. Hilse, M. Schlages, and D. O. Gericke, *Phys. Rev. E* **77**, 056404 (2008).
- [45] J. M. J. van Leeuwen, J. Groeneveld, and J. de Boer, *Physica* **25**, 792 (1959).
- [46] J. De Boer, J. M. J. Van Leeuwen, and J. Groeneveld, *Physica* **30**, 2265 (1964).
- [47] J. P. Hansen and I. R. McDonald, *Theory of Simple Liquids*, 3rd ed. (Elsevier, London/Burlington, MA, 2006).
- [48] H. Iyetomi, S. Ogata, and S. Ichimaru, *Phys. Rev. A* **46**, 1051 (1992).
- [49] A. Diaw and M. S. Murillo, *Astrophys. J.* **829**, 16 (2016).
- [50] Y. Hou, Y. Jin, P. Zhang, D. Kang, C. Gao, R. Redmer, and J. Yuan, *Matter Radiat. Extrem.* **6**, 026901 (2021).
- [51] E. M. Lifshitz and L. P. Pitaevskii, *Physical Kinetics* (Pergamon Press, Oxford, 1981).
- [52] A. Decoster, P. A. Markowich, B. Perthame, and P.-A. Raviart, *Modeling of collisions*, Series in Applied Mathematics (Gauthier-Villars, Paris, 1998).
- [53] L. G. Stanton and M. S. Murillo, *Phys. Rev. E* **93**, 043203 (2016).
- [54] G. Kagan and X.-Z. Tang, *Phys. Lett. A* **378**, 1531 (2014).
- [55] J. D. Huba, *2013 NRL Plasma Formulary* (Naval Research Laboratory, Washington, D.C., 2013).
- [56] J. Daligault, *Phys. Rev. Lett.* **96**, 065003 (2006).
- [57] S. Bastea, *Phys. Rev. E* **71**, 056405 (2005).
- [58] R. M. More, *Adv. At. Mol. Phys.* **21**, 305 (1985).
- [59] B. Boates and S. A. Bonev, *Phys. Rev. Lett.* **102**, 015701 (2009).
- [60] N. Smith, *Phys. Rev. B* **64**, 155106 (2001).
- [61] K. P. Driver and B. Militzer, *Phys. Rev. B* **93**, 064101 (2016).
- [62] K. P. Driver, F. Soubiran, S. Zhang, and B. Militzer, *J. Chem. Phys.* **143**, 164507 (2015).
- [63] R. S. McWilliams, D. A. Dalton, M. F. Mahmood, and A. F. Goncharov, *Phys. Rev. Lett.* **116**, 255501 (2016).
- [64] L. E. Crandall, J. R. Rygg, D. K. Spaulding, T. R. Boehly, S. Brygoo, P. M. Celliers, J. H. Eggert, D. E. Fratanduono, B. J. Henderson, M. F. Huff, R. Jeanloz, A. Lazicki, M. C. Marshall, D. N. Polsin, M. Zaghoo, M. Millot, and G. W. Collins, *Phys. Rev. Lett.* **125**, 165701 (2020).
- [65] R. Kubo, *J. Phys. Soc. Jpn.* **12**, 570 (1957).
- [66] D. A. Greenwood, *Proc. Phys. Soc.* **71**, 585 (1958).